The Journal of Chemical Physics ARTICLE pubs.aip.org/aip/jcp

A new parameterization of the DFT/CIS method with applications to core-level spectroscopy

Cite as: J. Chem. Phys. 161, 044114 (2024); doi: 10.1063/5.0220535
Submitted: 26 May 2024 • Accepted: 8 July 2024 •
Published Online: 25 July 2024

Aniket Mandal,[1] Eric J. Berquist,[2,a)] and John M. Herbert[1,b)]

AFFILIATIONS

[1] Department of Chemistry and Biochemistry, The Ohio State University, Columbus, Ohio 43210, USA
[2] Q-Chem Inc., Pleasanton, California 94588, USA

[a)] **Present address:** Sandia National Laboratories, Albuquerque, New Mexico 87185, USA.
[b)] **Author to whom correspondence should be addressed:** herbert@chemistry.ohio-state.edu

ABSTRACT

Time-dependent density functional theory (TD-DFT) within a restricted excitation space is an efficient means to compute core-level excitation energies using only a small subset of the occupied orbitals. However, core-to-valence excitation energies are significantly underestimated when standard exchange–correlation functionals are used, which is partly traceable to systemic issues with TD-DFT's description of Rydberg and charge-transfer excited states. To mitigate this, we have implemented an empirically modified combination of configuration interaction with single substitutions (CIS) based on Kohn–Sham orbitals, which is known as "DFT/CIS." This semi-empirical approach is well-suited for simulating x-ray near-edge spectra, as it contains sufficient exact exchange to model charge-transfer excitations yet retains DFT's low-cost description of dynamical electron correlation. Empirical corrections to the matrix elements enable semi-quantitative simulation of near-edge x-ray spectra without the need for significant *a posteriori* shifts; this should be useful in complex molecules and materials with multiple overlapping x-ray edges. Parameter optimization for use with a specific range-separated hybrid functional makes this a black-box method intended for both core and valence spectroscopy. Results herein demonstrate that realistic K-edge absorption and emission spectra can be obtained for second- and third-row elements and 3*d* transition metals, with promising results for L-edge spectra as well. DFT/CIS calculations require absolute shifts that are considerably smaller than what is typical in TD-DFT.

I. INTRODUCTION

More often than not, electronic structure theory is a balancing act. Users must choose between high accuracy at crippling computational cost (as exemplified by coupled-cluster theory or complete active space methods) or low cost at the expense of accuracy (Hartree–Fock theory). Density-functional theory (DFT) occupies a middle space where good accuracy is often possible at low cost, yet robustness and systematic improvability are sacrificed. To achieve a better balance of cost vs accuracy, there is interest in amalgamating correlated wave function models with DFT,[1–8] using the latter to capture dynamical electron correlation at low cost but combining this with a multiconfigurational wave function treatment that captures static correlation.

A simple first step along these lines is the "DFT/CIS" method, originally introduced by Grimme,[9] which uses molecular orbitals (MOs) from Kohn–Sham theory within a modified form of configuration interaction with single substitutions (CIS). The use of Kohn–Sham eigenvalues within the CIS formalism leads to more accurate excitation energies as compared to CIS itself, as orbital energy gaps are modeled more accurately, yet the CIS formalism is free of self-interaction problems that sometimes plague time-dependent (TD-)DFT.[10] The DFT/CIS approach has been extended to multireference CI wave functions (DFT/MRCI),[11] and that approach is experiencing something of a revival.[4,12–21] The CIS-based version still offers some attractive features, however, including an integral-direct formulation that is extremely efficient for large systems[22–26] and restricted open-shell formulations that can achieve correct multiplet structure.[27–29]

In the present work, we extend the parameterization of DFT/CIS to facilitate its use in x-ray absorption near-edge spectroscopy (XANES),[30] including core-level excitations of transition metal elements. Metal pre-edge features are particularly informative,[31–35] and time-dependent density functional theory

(TD-DFT) is a popular method for simulating metal pre-edge x-ray spectra. As usual for TD-DFT, excitation energies are sensitive to the choice of exchange–correlation (XC) functional, even as compared to ground-state properties.[10] Core-level excitation energies are significantly shifted relative to the experiment, with errors of $\gtrsim 10$ eV for second-row elements[36–39] and even larger for heavier elements.[39–41] Although peak splittings and chemical shifts are preserved to much greater accuracy, often rivaling that of correlated wave function methods,[42] the need for large *a posteriori* shifts can make it difficult to identify elemental edges in cases where multiple edges overlap.[26]

The present work introduces a reparameterization of the DFT/CIS method that is appropriate for both valence and core-level spectroscopy, where only the former has been previously considered in this context. Our parameterization is based on a range-separated hybrid functional and extends the semi-empirical shifts in the CIS matrix elements to include core levels of elements beyond Ne. For XANES applications, we have implemented DFT/CIS using a core/valence separation (CVS) approximation. This approach, which is sometimes called TD-DFT with a restricted excitation window, amounts to using an active space consisting of a few occupied orbitals of interest (core states) along with the full virtual space.[26,43] The present work focuses on elemental K-edge excitations, meaning those originating from 1*s* orbitals. These transitions are not affected by multiplet problems, so a restricted open-shell formulation is unnecessary, and the effect of spin–orbit coupling is negligible. These extensions can be pursued in due course, but the present work demonstrates that DFT/CIS affords a balanced description of both valence and core-level excitation energies while eliminating large systematic errors in the latter. DFT/CIS can thus be regarded as a (semi-empirical) black-box approach to computational electronic spectroscopy, from core to valence.

II. THEORY

A. DFT/CIS

The DFT/CIS formalism is very similar to CIS, with a few important modifications necessitated by the use of Kohn–Sham orbitals. Our notation is that $\psi_i, \psi_j, \ldots$ denote occupied MOs and $\psi_a, \psi_b, \ldots$ are virtual MOs, with indices $r, s, \ldots$ referring to arbitrary MOs. The quantity $|\Psi_i^a\rangle$ represents a singly substituted Slater determinant constructed from a reference determinant $|\Psi_0\rangle$ that is the solution to the self-consistent field (SCF) problem. Using a closed-shell formalism for simplicity (although our implementation includes the spin-unrestricted case), the matrix elements of the CIS Hamiltonian are[9]

$$\langle \Psi_i^a | \hat{H} | \Psi_i^a \rangle = E_0 + \left(\psi_a \middle| \hat{f} \middle| \psi_a \right) - \left(\psi_i \middle| \hat{f} \middle| \psi_i \right) - (\psi_i \psi_i | \psi_a \psi_a) + 2(\psi_i \psi_a | \psi_i \psi_a), \tag{1a}$$

$$\langle \Psi_0 | \hat{H} | \Psi_i^a \rangle = \sqrt{2} \left(\psi_i \middle| \hat{f} \middle| \psi_a \right), \tag{1b}$$

and

$$\langle \Psi_i^a | \hat{H} | \Psi_j^b \rangle = \left(\psi_a \middle| \hat{f} \middle| \psi_b \right) \delta_{ij} - \left(\psi_i \middle| \hat{f} \middle| \psi_j \right) \delta_{ab} - (\psi_i \psi_j | \psi_a \psi_b) + 2(\psi_i \psi_a | \psi_j \psi_b). \tag{1c}$$

The quantity E_0 is the ground-state energy, and $\hat{f}$ is the Fock operator. Two-electron integrals are expressed in Mulliken notation, and Eq. (1) does not assume that the MOs are canonical. If they are, then

$$\left(\psi_r \middle| \hat{f} \middle| \psi_s \right) = \varepsilon_r \delta_{rs}. \tag{2}$$

In Grimme's DFT/CIS method,[9] the matrix elements in Eq. (1) are modified as follows:

$$\langle \Psi_i^a | \hat{H} | \Psi_i^a \rangle = E_0 + \varepsilon_a^{\mathrm{KS}} - \varepsilon_i^{\mathrm{KS}} + 2J_{ia} - c_1 K_{ia} + \Delta J_{ia}(\varepsilon_{ia}), \tag{3a}$$

$$\langle \Psi_0 | \hat{H} | \Psi_i^a \rangle = 0, \tag{3b}$$

and

$$\langle \Psi_i^a | \hat{H} | \Psi_j^b \rangle = 2(\psi_i \psi_a | \psi_j \psi_b) - c_1 (\psi_i \psi_j | \psi_a \psi_b). \tag{3c}$$

In this case, E_0 in Eq. (3a) is the Kohn–Sham ground-state energy and the quantities $\{\psi_r\}$ and $\{\varepsilon_r^{\mathrm{KS}}\}$ are the Kohn–Sham MOs and their energy levels, respectively. The quantities J_{ia} and K_{ia} in Eq. (3a) are the Coulomb and exchange integrals,[44,45] respectively, evaluated using Kohn–Sham MOs. Equation (3b) is a Brillouin-like condition that is invoked by fiat. Empirical corrections that appear in the matrix elements of Eq. (3a) are discussed below, specifically the parameter c_1 and the function $\Delta J_{ia}(\varepsilon_{ia})$.

The DFT/CIS approach proves beneficial because the Kohn–Sham eigenvalue gaps $\varepsilon_a^{\mathrm{KS}} - \varepsilon_i^{\mathrm{KS}}$ are approximations to excitation energies in a way that their Hartree–Fock counterparts (which are typically much larger) are not.[46–48] This leads to less configuration mixing in the excited state.[49] In part, this is due to the fact that Kohn–Sham calculations often result in one or more bound virtual orbitals ($\varepsilon_a < 0$), even when approximate XC functionals are used, whereas Hartree–Fock virtual orbitals are often all unbound. In the latter case, significant configuration mixing is required in order to obtain localized excited states from discretized continuum orbitals.[49,50]

Unlike the working equations for linear-response TD-DFT,[10] the matrix elements in Eq. (3) do not contain an XC kernel but are instead CIS-like, albeit with empirical parameters added to the diagonal matrix elements in Eq. (3a). These include a scaling-down of the exchange integral, for which Grimme uses the value $c_1 = 0.317$.[9] This parameter compensates for the semilocal DFT exchange that is included in the SCF calculation that is used to obtain the MOs. A shift is also added to the diagonal elements, of the form[9]

$$\Delta J(\varepsilon) = -0.025\varepsilon + c_2 \exp(-c_3 J^4). \tag{4}$$

This correction was added to deal with Rydberg-type excited states, where the Coulomb integral is small. (For cases of orbital degeneracy, it is suggested to average J over the degenerate configurations to avoid symmetry breaking,[9] but our implementation does not do this.) In addition to $c_1 = 0.317$, parameters $c_2 = 0.033 E_{\mathrm{h}}$ and $c_3 = 1.27 \times 10^7\ E_{\mathrm{h}}^{-4}$ in Eq. (4) were determined by Grimme,[9] specifically for use with the B3LYP functional.[51,52] Grimme's implementation also uses a custom basis set that is described in Sec. III C. The DFT/CIS method is intended as a semi-empirical approach that is tied specifically to this particular XC functional and basis set.

B. Reparameterization

For the present work, we have implemented Grimme's original parameterization, and we will refer to it as B3LYP/CIS. Our implementation reproduces the results published in Ref. 9 when used with the custom basis set described in that work.

In attempting to use B3LYP/CIS for core-level spectroscopy, however, it became clear that the shifts in Eq. (4) are not appropriate beyond the second row of the periodic table (i.e., beyond Ne). As such, we decided to revisit the parameterization of Eq. (3a). In the time since the original formulation of DFT/CIS, range-separated hybrid functionals[10,53,54] have proven to be some of the most effective XC functionals for TD-DFT;[10] hence, our new parameterization is based on a range-separated counterpart of B3LYP known as CAM-B3LYP.[55] We refer to this new parameterization as CAM-B3LYP/CIS, and we have developed it for use with a standard Gaussian basis set, def2-TZVPD.[56,57]

For CAM-B3LYP/CIS, we modify Eq. (3a) to be

$$\left\langle \Psi_i^a \middle| \hat{H} \middle| \Psi_i^a \right\rangle = E_0 + \varepsilon_a^{\mathrm{KS}} - \varepsilon_i^{\mathrm{KS}} + 2c_2 J_{ia} - c_1 K_{ia} - \Delta\varepsilon, \tag{5}$$

while keeping Eqs. (3b) and (3c) the same. Parameters $c_1 = 0.525$ and $c_2 = 0.850$ were determined using a subset of the QuestDB data set,[58] consisting of benchmark excitation energies for 18 small to medium-sized molecules.

The correction $\Delta\varepsilon$ is taken to be

$$\Delta\varepsilon = \begin{cases} +0.0250\varepsilon & \text{if } |\varepsilon| \le 102\ E_{\mathrm{h}}, \\ +0.0083\varepsilon - 1.4209\ E_{\mathrm{h}} & \text{if } |\varepsilon| > 102\ E_{\mathrm{h}}. \end{cases} \tag{6}$$

This was determined by fitting CAM-B3LYP orbital energies to those obtained using the short-range corrected (SRC) functional known as SRC1.[38,39,59] (See Fig. S1 for the data.) The SRC1 functional was specifically parameterized to obtain TD-DFT core-level spectra with experimental accuracy. In other words, rather than shifting spectra with respect to the experiment (as is required in TD-DFT calculations using B3LYP or CAM-B3LYP), we shift the ground-state core orbital energies obtained from CAM-B3LYP to match the corresponding SRC1 values. Our aim is to reduce the inherent errors in core-level eigenvalues obtained from CAM-B3LYP. Absent the $\Delta\varepsilon$ correction, self-interaction error (SIE) in CAM-B3LYP leads to orbital energies that are less strongly bound as compared to SRC1 values. The latter functional uses a large fraction of exact exchange on a very short length scale (<1 Å) in order to reduce SIE in the core states.[38]

For elements through Ne, the shift introduced in Eq. (6) for $|\varepsilon| \le 102E_{\mathrm{h}}$ is essentially the same as what is used in Grimme's B3LYP-based implementation, because core-level eigenvalues from both B3LYP and CAM-B3LYP underestimate excitation energies for x-ray absorption by approximately the same amount. The present work extends the parameterization to third-row elements ($|\varepsilon| > 102E_{\mathrm{h}}$). Our choice for the modifications in Eqs. (5) and (6) is motivated by the observation that the majority of the correction in B3LYP/CIS comes from the c_1 parameter. The exponential correction in Eq. (4) that is used in B3LYP/CIS was introduced by Grimme in order to deal with Rydberg and charge-transfer states where the Coulomb integral J_{ia} is much smaller than it is compared for localized valence excitations, but the dependence on the Coulomb integral J in Eq. (4) is inconvenient from an implementation perspective. Range separation in the CAM-B3LYP functional equips this method to better account for charge-separated states as compared to B3LYP, so the more complicated form of $\Delta J(\varepsilon)$ was avoided in our re-parameterization.

C. Core-level spectroscopy with DFT/CIS

Conventional TD-DFT can be used to describe the x-ray near-edge region, involving transitions from core MOs to the lowest unoccupied MO (LUMO) and other low-lying virtual orbitals. However, core excitation energies are systematically underestimated (i.e., insufficiently bound) when computed using either generalized gradient approximations (GGAs) or hybrid functionals.[38,48,60,61] Errors increase with the atomic number of the element in question.[41] One way of tackling this problem is simply to shift the calculated TD-DFT spectra,[35] since the relative energies of different spectral features are much more accurate than the absolute excitation energies,[42] although this can be problematic in systems with multiple overlapping elemental edges, especially where heavier elements are involved.[26] Adjusting the fraction of exact exchange in the XC functional can reduce the need for empirical shifting,[38,41] although large fractions ($\gtrsim$ 50% Hartree–Fock exchange) are often necessary.[38,62] To avoid this, Besley and coworkers parameterized SRC1 and related functionals specifically for core-level spectroscopy.[38,59] These functionals use range separation, in conjunction with the short-range μBLYP exchange functional,[53,63] to apply a large fraction of exact exchange on a length scale of <1 Å. The SRC functionals accurately reproduce elemental K-edge excitation energies but perform quite poorly in ΔSCF calculations,[64,65] suggesting that their success rests mostly on error cancellation.

The use of specific density functionals calls into question the black-box nature of TD-DFT. If we are to rely on specific functionals anyway, then the functional-specific parameterization of DFT/CIS does not seem like much of an additional limitation and may actually be an advantage insofar as DFT/CIS may provide a balanced description of both core and valence excitations within a single method. (Functionals with 50% Hartree–Fock exchange exhibit larger errors for valence excitation energies as compared to the current state-of-the-art in TD-DFT.[10]) Moreover, DFT/CIS has a specific advantage over TD-DFT when it comes to calculating core-excitation spectra due to its treatment of Rydberg and charge-transfer states. Long-range corrected (LRC) functionals,[10,53,54,66] based on range separation, can accurately describe both valence, Rydberg, and charge-transfer excitation energies.[66] However, core-excitation energies remain too low,[67] due to the absence of a large fraction of exact exchange at short range, leading to differential SIE between the core and valence orbitals. Note that the c_1 parameter in DFT/CIS adds Hartree–Fock exchange to the CIS matrix elements.

D. X-ray emission using DFT/CIS

Accurate valence-to-core x-ray emission (XES) spectra have previously been simulated using Slater's transition method[64] and also at the level of equation-of-motion coupled-cluster theory using a reference state containing a core hole.[68] In the latter case, however, the coupled-cluster amplitude equations can

sometimes be difficult to converge.[69,70] (The core hole can cause problems for perturbation theory as well.[71,72]) The analogous procedure is much more robust when used with TD-DFT.[73–75] It can be extended to DFT/CIS using the following procedure:

1. Perform a normal DFT calculation on the neutral ground state of the molecule in question. The functional (B3LYP or CAM-B3LYP) and basis set should be appropriate for DFT/CIS.
2. Use the Kohn–Sham MOs thus obtained as a starting point to optimize a core-ionized reference state. To do so, one should use a convergence algorithm designed for non-*Aufbau* Slater determinants,[10,76–78] in order to prevent collapse of the core hole during the SCF iterations.
3. Perform a standard DFT/CIS calculation atop the core-excited reference state. The XES transitions appear as negative excitation energies, with negative oscillator strengths f_{0n} due to the appearance of negative excitation frequencies $\omega_{n0} = (E_n - E_0)/\hbar$ in the formula[10]

$$f_{0n} = \left(\frac{2m_e\omega_{n0}}{3e^2\hbar}\right)\|\langle 0|\hat{\boldsymbol{\mu}}|n\rangle\|^2. \tag{7}$$

Importantly, no additional SCF cycles should be performed on the ionized core-hole reference state if it is read in from a separate job between steps 2 and 3.[79] (Additional Roothaan steps are sometimes used to ensure the consistency of the Fock and density matrices for a set of input orbitals,[79] but in the present context this spoils the core-hole reference state and degrades the quality of the XES spectra simulated using TD-DFT.) This approach corresponds to a "sudden" approximation,[30] in which MOs for the neutral molecule are used to describe the ionized core-hole state.

III. COMPUTATIONAL DETAILS

The DFT/CIS method has been implemented in the Q-Chem program and is available starting with v. 6.2.[80] We focus on K-edge excitation spectra in the present work in order to evaluate the accuracy and efficacy of DFT/CIS for x-ray spectroscopy. These spectra are less complicated to simulate as compared to L- or M-edge spectra because relativistic and spin–orbit coupling effects are small[64] and because there is little interaction with valence occupied orbitals so that the CVS approximation is accurate and robust.[26,81]

For some second-row elements and 3*d* transition metals, we add an atomic relativistic correction to the TD-DFT and DFT/CIS excitation energies. Following Besley and co-workers,[73,82,83] these scalar shifts are computed as the difference in relativistic Douglas–Kroll–Hess[84–86] and non-relativistic Hartree–Fock energy levels, for 1*s* orbitals of the isolated atoms, computed using the cc-pVQZ-DK basis set.[87] These calculations were performed using NWChem.[88]

A. Core/valence separation

The CVS approximation extends standard excited-state methods to core-level states by eliminating the amplitudes associated with all but a small number of occupied MOs.[26,43] This reduces the computational cost drastically and separates the highly excited core states from the continuum. It also allows the separation of K-edge spectra from L- and M-edge spectra. For the K-edge spectra examined here, the CVS active space consists of the 1*s* orbitals for the element in question, along with the entire virtual space. All core-level TD-DFT and DFT/CIS calculations reported here invoke the CVS approximation, which affords negligible errors for K-edge spectra.[26] In molecules containing more than one atom with the same atomic number, all of the 1*s* orbitals for the element in question are included in the active space.

Conventional TD-DFT calculations reported here also use the CVS approximation along with the Tamm–Dancoff approximation,[10,49] which is consistent with the CIS-style matrix elements used in DFT/CIS. The Tamm–Dancoff approximation affords negligible errors for K-edge excitation energies.[26]

B. XC functionals

DFT/CIS calculations were performed using either B3LYP[51,52] or CAM-B3LYP.[55] The XC functionals themselves have not been modified; all of the new or modified parameters for DFT/CIS are contained in the modified CIS-style equations that are discussed in Sec. II A. The B3LYP/CIS method represents Grimme's original parameterization in Eq. (3),[9] while CAM-B3LYP/CIS is the new parameterization given by Eq. (5).

As a point of comparison, conventional TD-DFT calculations are also reported using the same two functionals, B3LYP and CAM-B3LYP. In addition, we report TD-DFT calculations using the SRC1-r1 and SRC1-r2 functionals.[38,59] These two functionals are intended for use with second-row atoms (r1) or third-row atoms (r2), respectively.

TD-SRC1 excitation energies are used as reference values in this work because that method was specifically parameterized to reproduce experimental K-edge excitation energies and works very well in that capacity.[26,38,39,59] These functionals use a large fraction of exact exchange ($\gtrsim$50%) at short range, in order to reduce differential self-interaction errors between occupied core and valence-virtual MOs. As a further point of comparison, we report TD-BH&HLYP calculations.[89] That functional uses 50% Hartree–Fock exchange without range separation.

C. Basis sets

B3LYP/CIS calculations reported here use a bespoke basis set introduced by Grimme for this purpose.[9] Its construction starts from the valence triple-zeta (VTZ) basis set introduced by Ahlrichs and co-workers,[90] then adds additional polarization functions: *d*-functions on carbon and *p*-functions on hydrogen, each with $\zeta = 0.8\ a_0^{-2}$.[9] For Rydberg states, this basis set was augmented with one set of diffuse *sp*-functions on each non-hydrogen atom, with exponents selected according to Dunning's procedure.[91] This basis set will be denoted as "VTZ+" and its complete specification is provided in the supplementary material.

CAM-B3LYP/CIS parameters were developed based on calculations using the def2-TZVPD basis set,[57] which should be converged for CIS and TD-DFT excitation energies.[10,92–96] Unless otherwise specified, CAM-B3LYP/CIS calculations use this basis set, as do conventional TD-DFT calculations reported here. Some examples are provided of CAM-B3LYP/CIS calculations using the def2-SVPD

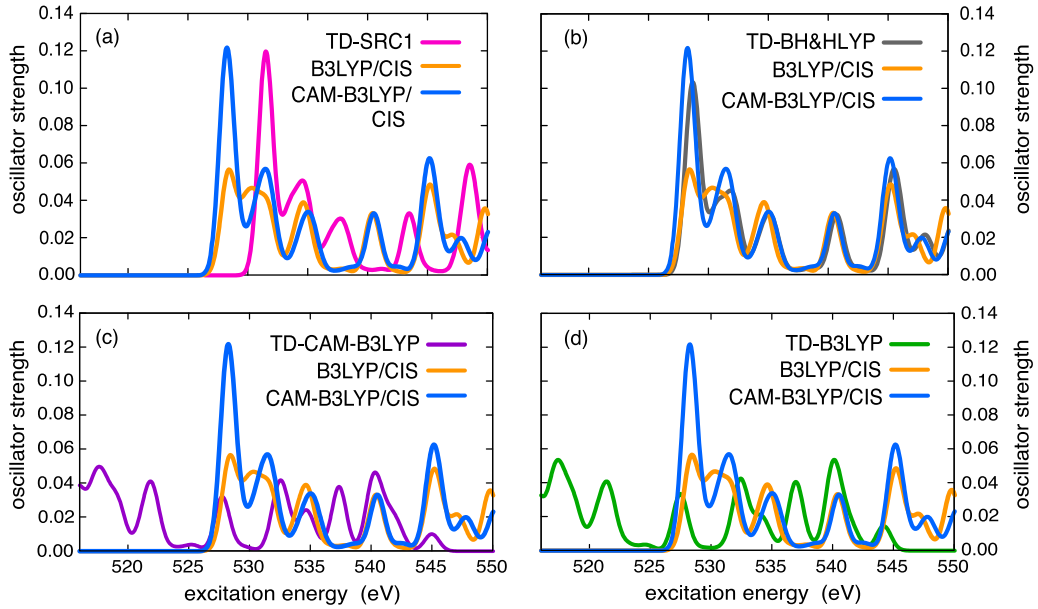

FIG. 1. Simulated K-edge absorption of TiO_2 obtained using two different parameterizations of DFT/CIS, as compared to conventional TD-DFT using the functionals (a) SRC1-r1, (b) BH & HLYP, (c) CAM-B3LYP, and (d) B3LYP. The two DFT/CIS spectra are the same in each panel and serve as reference spectra that highlight how sensitive the TD-DFT spectrum is to the fraction of Hartree–Fock exchange. TD-DFT and CAM-B3LYP/CIS calculations use the def2-TZVPD basis set whereas B3LYP/CIS calculations use the VTZ+ basis set.

and def2-SV(P) basis sets,[56,57] in an effort to gauge whether the parameterization is sensitive to the choice of basis set.

IV. RESULTS AND DISCUSSION

A. Role of Hartree–Fock exchange

DFT/CIS and TD-DFT spectra for an isolated formula unit of TiO_2 are presented in Fig. 1 at the oxygen K edge, using several related functionals with differing amounts of Hartree–Fock exchange. Near-edge features obtained using TD-B3LYP [Fig. 1(d)] are off by about 16 eV relative to the experimental edge at 531 eV.[97] TD-CAM-B3LYP does not rectify this in any significant way [Fig. 1(c)], whereas TD-SRC1-r1 affords the correct value [Fig. 1(a)]. Using the latter as a stand-in for the experimental K-edge and comparing it to either parameterization of DFT/CIS [Fig. 1(a)], one observes that the DFT/CIS near-edge peaks differ by about 1.9 eV. On the other hand, the DFT/CIS excitation energies are nearly an exact match to those obtained using TD-BH&HLYP [Fig. 1(b)], which was certainly not built into the parameterization. This tells us that the absolute accuracy of the K-edge ($1s \rightarrow$ LUMO excitation) depends sensitively on the fraction of exact exchange. A pronounced intensity difference between B3LYP/CIS and CAM-B3LYP/CIS is primarily due to inadequacies of the custom VTZ+ basis set that is used in B3LYP/CIS. For that reason, we rejected VTZ+ for the new parameterization, opting instead for an up-to-date choice, namely, def2-TZVPD.

In critiquing the 1.9 eV error for DFT/CIS, it is worth comparing the performance of conventional TD-DFT as a baseline. Using a functional $B^{x}LYP$ with a variable fraction (x) of Hartree–Fock exchange, Besley *et al.*[38] demonstrated that $x = 0.57$ performs much better in terms of absolute accuracy as compared to B3LYP with $x = 0.20$. The mean errors for the $B^{0.57}LYP$ functional were reported to be 0.7 eV for core-to-valence transitions of second-row elements and 0.9 eV for core-to-Rydberg excitations, whereas the corresponding TD-B3LYP errors are 12.7 eV (core → valence) and 12.9 eV (core → Rydberg).[38]

Our own benchmarks, using the Quest1 data set,[58] afford a mean absolute error of 0.28 eV for valence excitation energies, essentially identical to the ~0.3 eV accuracy that was reported in the original implementation, using a much smaller data set.[9] This should be compared to CIS itself, where average errors are $\gtrsim 1$ eV.[10] (Keep in mind that there is no XC kernel in the DFT/CIS matrix elements.) We plan to provide a more thorough assessment of DFT/CIS for valence excitation energies in due course, but preliminary data suggest that this method is no worse than TD-B3LYP, which remains one of the best XC functionals for localized valence excitation energies.[10] At the same time, both DFT/CIS methods significantly outperform TD-B3LYP and TD-CAM-B3LYP for core excitations, as discussed at greater length below.

B. Benchmarking core excitation energies

Both parameterizations of DFT/CIS have a core correction that works very well for second-row elements (through Ne), offsetting errors in the Kohn–Sham eigenvalues for core states. Table I illustrates the accuracy for K-edge excitations ($1s \rightarrow$ LUMO) of the elements carbon, oxygen, and nitrogen in comparison to theoretical best estimates of the excitation energies that were compiled in Ref. 19

TABLE I. Errors in excitation energies for elemental K-edge transitions in comparison to benchmark values.

		Error (eV)[a]							
			DFT/CIS		TD-DFT[b]				
Molecule	Element	CIS	CAM-B3LYP[c]	B3LYP[d]	CAM-B3LYP	B3LYP	SRC1-r1	DFT/MRCI[e]	ΔE (eV)[f]
Acetaldehyde	C	9.82	−4.64	−3.46	−9.98	−9.94	0.58	−2.82	286.30
Acetaldehyde	O	20.82	1.33	1.81	−10.93	−11.08	4.53	2.00	531.14
Acetic acid	C	8.47	−5.24	−3.59	−13.22	−10.07	0.02	−2.75	288.69
Acetic acid	O	18.14	−1.73	−0.99	−13.53	−13.68	1.63	−2.51	531.95
Acetone	C	7.69	−2.46	−4.70	−11.15	−11.06	−0.86	−4.11	286.80
Acetone	O	15.28	−3.52	−2.22	−14.52	−14.58	−0.11	−3.69	531.30
Benzaldehyde	C	6.93	−7.28	−6.06	−12.61	−12.64	−2.18	−5.31	287.70
Benzaldehyde	O	15.45	−3.41	1.95	−14.52	−14.72	−0.06	−4.32	531.00
Benzamide	C	6.84	−7.52	−6.73	−13.25	−13.87	−0.80	−3.95	288.09
Dimethyl carbonate	C	7.48	−6.20	−4.52	−12.57	−11.71	−0.85	−3.32	290.33
Dimethyl carbonate	O	23.37	−2.99	0.85	−11.90	−12.03	4.30	−2.86	532.93
Diphenyl carbonate	O	22.02	−3.13	1.10	−11.35	−11.48	4.09	−0.95	532.93
Diphenyl urea	O	16.69	−2.97	−2.20	−14.59	−14.99	0.32	−1.59	532.50
Terephthaldehyde	C	6.42	−7.84	−6.64	−13.21	−14.75	−3.30	−6.12	288.20
Terephthaldehyde	O	19.80	−0.45	−0.96	−12.93	−14.09	1.79	−4.58	530.60
Urea	C	7.67	−6.06	−4.41	−10.86	−10.80	−0.74	−3.30	289.53
Urea	O	17.12	−2.62	−1.80	−14.23	−14.34	0.83	−2.56	532.50
Phenylalanine	N	15.17	−1.76	−2.28	−12.74	−11.66	0.92	−2.15	401.20
Phenylalanine	O	15.93	−3.20	−2.07	−11.91	−14.53	0.22	−3.38	532.20
Tyrosine	C	10.15	2.91	−3.93	−10.44	−10.63	−0.35	3.44	285.10
MAE[g]	⋯	13.56	3.86	3.15	12.52	12.63	1.43	3.29	

[a]Relative to the theoretical best estimate (ΔE) in the final column.
[b]Tamm–Dancoff approximation, def2-TZVPD basis set.
[c]Parameterization introduced in the present work, def2-TZVPD basis set.
[d]Parameterization from Ref. 9, VTZ+ basis set.
[e]From Ref. 19.
[f]Theoretical best estimates from Ref. 19.
[g]Mean absolute errors, relative to theoretical best estimates.

from various sources.[98–105] TD-CAM-B3LYP, TD-B3LYP, and TD-SRC1-r1 results are also included, as are DFT/MRCI values from Ref. 19.

DFT/MRCI is a multireference extension of DFT/CIS, with similar underlying principles but different modifications to the matrix element and no explicit core orbital energy correction. Both methods exhibit similar errors, suggesting that the multireference nature of DFT/MRCI is unnecessary for these examples. However, this similarity also suggests that the multireference *ansatz* and/or the double excitations effectively compensate for the SIE, avoiding the need for large scalar shifts.

The two DFT/CIS methods afford consistently larger errors at the carbon K-edge as compared to the oxygen K-edge. This results from the $\Delta\varepsilon$ correction in Eq. (6), where $\Delta\varepsilon = 0.025\varepsilon$ is a somewhat better correction for oxygen than it is for carbon. In our view, these slightly larger errors for carbon (and, in certain cases, for nitrogen) are not large enough to warrant reparameterization. The present version improves upon both uncorrected CIS and also TD-DFT (using the same functionals) by ∼10 eV. The shift $\Delta J(\varepsilon)$ in Eq. (4) matches $\Delta\varepsilon$ very well for second-row elements, so results for B3LYP/CIS are similar to those for CAM-B3LYP/CIS.

Note the comparison between mean absolute errors (MAEs) in Table I, which are assessed relative to theoretical best estimates of the transition energies. Conventional TD-B3LYP and TD-CAM-B3LYP calculations improve upon conventional CIS by ∼1 eV, which is similar to what is observed for valence excitation energies,[10] yet this is much smaller than the ∼10 eV improvement for DFT/CIS. This suggests that most of the improvement in the DFT/CIS case comes from the shift $\Delta\varepsilon$ or $\Delta J(\varepsilon)$. In other words, most of the error in TD-DFT excitation energies for K-edge transitions comes from an error in the 1*s* eigenvalues. At the same time, we note that CIS errors are opposite in sign from those obtained using TD-B3LYP and TD-CAM-B3LYP, with CIS overestimating every single K-edge excitation energy while these two TD-DFT methods underestimate every single one. Since there is no SIE in the Hartree–Fock eigenvalues, these discrepancies in the CIS case must result from a lack of sufficient orbital relaxation, with only ∼1 eV of the error arising from missing electron correlation. The fact that the TD-(CAM-)B3LYP errors in K-edge energies range from −10 eV to −15 eV, while also missing orbital relaxation, suggests that the SIE in 1*s* orbital energies likely exceeds 20 eV.

TD-SRC1-r1 errors are much smaller than those obtained using TD-B3LYP or TD-CAM-B3LYP and are not uniform in sign. The

TABLE II. Errors in K-edge excitation energies for third-row elements and 3*d* transition metals as compared to atomic benchmarks. Relativistic corrections are tabulated separately but have been added to all values.

		Error (eV)					
		TD-DFT			DFT/CIS		
Molecule	Relativistic correction[a]	SRC1-r2	B3LYP	CAM-B3LYP	B3LYP	CAM-B3LYP	ΔE (eV)
SiH_4	4.50	1.55	−40.29	−40.19	8.21	4.57	1845.50[b]
PH_3	6.02	1.75	−44.61	−44.65	13.49	7.07	2145.80[c]
H_2S	7.89	1.81	−49.22	−49.31	17.50	10.09	2473.10[d]
CH_3Cl	10.22	3.28	−52.57	−52.50	23.23	7.77	2823.08[e]
Mn complex[f]	52.84	13.80	−82.43	−82.08	77.28	6.17	6552.12[g]
Fe complex[f]	62.67	18.57	−134.38	−133.62	91.61	11.28	7125.87[g]
Ni complex[f]	85.91	64.37	−112.12	−111.92	158.12	54.37	8347.42[g]
Cu complex[f]	99.75	17.15	−98.79	−98.79	120.82	11.63	8986.96[g]

[a]Atomic Douglas–Kroll–Hess/cc-pVQZ-DK, from the present work.
[b]Reference 106.
[c]Reference 107.
[d]Reference 108.
[e]Reference 109.
[f]See Fig. 2.
[g]Best estimates of the atomic K-edge transition (Ref. 110).

SRC1 functional was parameterized to reproduce K-edge transition energies of this sort, resulting in near-perfect cancellation of SIE (which tends toward underestimation of the excitation energy) and missing orbital relaxation (which increases the excitation energy).[62] The 52%:48% ratio of orbital relaxation to SIE, reported in Ref. 62 for TD-SRC1 calculations of core-level excitation energies, neatly encapsulates the balancing act between these competing sources of error.

The functional form of $\Delta\varepsilon$ changes for the third row of the periodic table [Eq. (6)]. Results for K-edge transition energies of heavier elements are presented in Table II, including molecules containing third-row elements Si, P, S, and Cl, along with a few organometallic complexes containing a 3*d* transition metal.[111–114] (These are shown in Fig. 2 and are taken from a much larger database of geometries for organometallic complexes.[115]) For the main-group molecules, results can be compared to experiments,[106–109] but for the 3*d* metal-containing systems we compare to K-edge excitation energies for the isolated metal atoms.[110] This is sufficient to estimate the overall shift that is required in a TD-DFT or DFT/CIS calculation. Relativistic Douglas–Kroll–Hess corrections are listed in Table II, and they are quite large for the 3*d* elements. These corrections have been added to the computed excitation energies in Table II as a post-processing step.

For CAM-B3LYP/CIS, errors are comparable in magnitude and have the same sign as errors obtained using TD-SRC1-r2, although both methods exhibit larger errors as compared to what we observed for second-row elements (Table I). Using B3LYP/CIS, the error is of the opposite sign to that of TD-B3LYP and is significantly larger than that of CAM-B3LYP/CIS, illustrating why B3LYP/CIS needed to be reparameterized for heavier elements. As discussed in Sec. II B, the formulation of CAM-B3LYP/CIS used TD-SRC1 reference data to parameterize $\Delta\varepsilon$, which is apparent in the fact that the two methods exhibit comparable errors that follow similar trends.

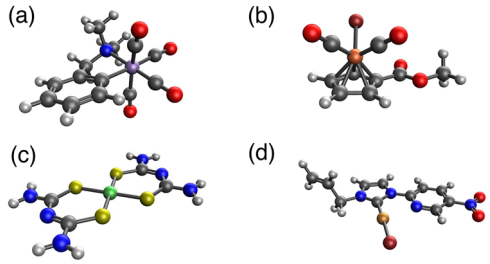

FIG. 2. Organometallic complexes considered in Table II: (a) tetracarbonyl(2-dimethylaminomethylphenyl)manganese,[111] (b) (η-$C_5H_4CO_2CH_3$)$Fe(CO)_2Br$,[112] (c) bis(dithiobitureto)Ni(II),[113] and (d) Cu(I)–N-heterocyclic carbene allyl (benzimidazolium) bromide.[114]

For these heavier elements, B3LYP/CIS consistently overestimates the excitation energies while CAM-B3LYP/CIS overestimates them, albeit to a lesser extent. This is particularly striking because the two methods employ corrections to the core-orbital energies that are similar in magnitude for second-row elements, illustrating the need for a row-specific correction. Either way, the errors are significantly smaller as compared to conventional TD-DFT with either B3LYP or CAM-B3LYP, by ~50 eV on average. For the transition metal complexes, CAM-B3LYP/CIS is slightly more accurate than TD-SRC1-r2.

C. Convergence studies on TiO_2 clusters

Neese and co-workers[116] have shown that reasonable agreement with experimental L- and M-edge XANES of bulk transition metal oxides and sulfides can be obtained using small cluster models, e.g., with only six Ti atoms to model solid-state TiO_2 or even one Fe

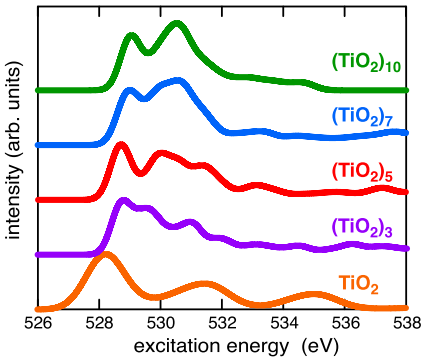

FIG. 3. Oxygen K-edge spectra computed using CAM-B3LYP/CIS for TiO_2 clusters with differing numbers of formula units. All spectra were computed using 1000 transition energies broadened using a Gaussian width of 0.3 eV. Each spectrum is scaled so that its most intense feature has unit intensity, thus the intensity scale can be compared across all five spectra.

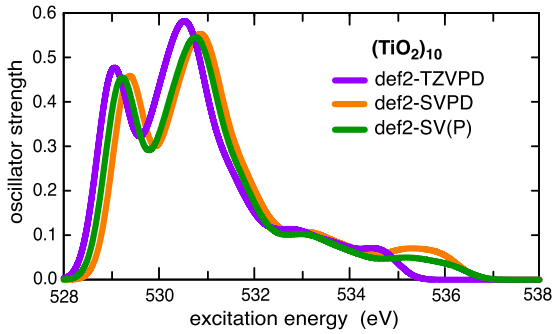

FIG. 4. Oxygen K-edge spectra for $(TiO_2)_{10}$, computed using CAM-B3LYP/CIS with different basis sets. All spectra were computed using 1000 transition energies broadened using a Gaussian width of 0.3 eV.

atom for solid-state FeS_2. To investigate convergence using the new CAM-B3LYP/CIS method, we examined TiO_2 clusters of varying size, up to 10 TiO_2 formula units. Oxygen K-edge spectra are shown in Fig. 3 and consist of two near-edge peaks representing excitations into t_{2g} and e_g MOs of the Ti($3d$) manifold. These peaks are well separated in the TiO_2 monomer but quickly converge as additional formula units are added, yet the relative intensities of these two features are reversed in larger clusters as compared to smaller ones. (Note that this is not an artifact of the finite number of excited states because it is the higher-energy peak that is more intense in larger clusters.) Peak positions and relative intensities appear to converge at $(TiO_2)_7$.

Figure 4 examines basis-set effects for CAM-B3LYP/CIS calculations using the largest of these clusters, $(TiO_2)_{10}$. The double-ζ basis sets def2-SV(P) and def2-SVPD result in a small (~2 eV) shift as compared to the def2-TZVPD basis set for which the method was parameterized, but the overall spectral shape is nearly identical. The def2-TZVP basis set affords a spectrum that is nearly indistinguishable from the one obtained using def2-TZVPD. This is not unique to DFT/CIS, and we have previously documented that core-level spectra computed using TD-DFT/double-ζ calculations are quite similar to results obtained in larger basis sets,[26] including those that contain core–valence polarization functions[117] or uncontracted primitive Gaussians,[82] which are intended to add variational flexibility in the description of the core hole. Meanwhile, def2-SV(P) speeds up the CAM-B3LYP/CIS calculation by ~23× as compared to def2-TZVPD. It appears that neither specialized basis sets nor basis sets of triple-ζ quality are warranted for XANES calculations using DFT/CIS or TD-DFT.

D. Strain effects in carbon-cage molecules

Absorption spectra at the carbon K-edge were reported recently for small diamondoid clusters,[118] three of which are investigated here: adamantane, twistane, and cubane (in order of increasing steric strain). The strain has an effect on the electronic structure of these clusters that has been investigated with the help of carbon K-edge spectra, and simulated spectra are juxtaposed with experimental spectra in Fig. 5. Note that the state-by-state (eigenstate-resolved) approach that is used here is not expected to capture the extended x-ray fine structure, which results from multiple scatterings of the outgoing electron,[30] but only the near-edge region that is characteristic of covalent bonding.

Experimental XANES spectra are characterized by a σ^*(C–C) resonance that splits from a broad peak into narrower peaks with increased strain, while the tertiary σ^*(C–H) peaks are broader for cubane with a shift to lower energies.[118] These essential near-edge features are well reproduced by CAM-B3LYP/CIS calculations [Fig. 5(b)], although the higher-energy peaks in cubane are shifted a bit too high in energy. TD-CAM-B3LYP spectra show similar features but require a shift of 11 eV to match experiment, as compared to 4 eV for CAM-B3LYP/CIS. Theoretical spectra for both adamantane and twistane show an intense feature around 290 eV, similar to that observed in various saturated hydrocarbons.[30] The shift relative to the K-edge is accurately reproduced by the CAM-B3LYP/CIS calculations. The largest differences between

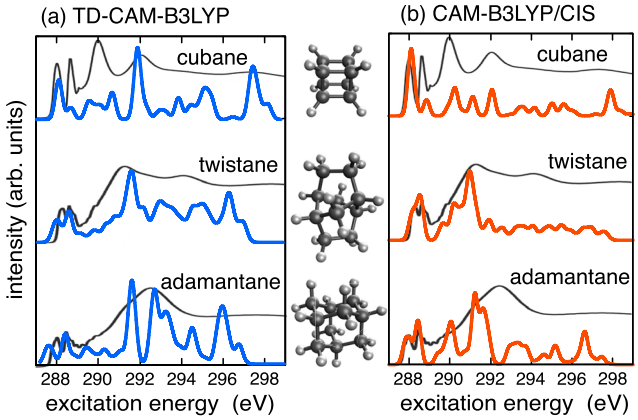

FIG. 5. Gas-phase K-edge spectra for small diamondoid cage molecules (as shown), computed using (a) TD-CAM-B3LYP and (b) CAM-B3LYP/CIS, compared to experimental spectra (in black) that are reproduced from Ref. 118. The simulated spectra include 600 vertical excitation energies broadened using a 0.15 eV Gaussian function. The TD-CAM-B3LYP spectra are shifted by 11 eV and the CAM-B3LYP/CIS spectra by 3.8 eV.

theory and experiment are observed for cubane, where two lower-energy features that are present around 287 eV for adamantane and twistane are not resolved in the simulated spectrum for cubane. (These features are associated with tertiary carbons and methylene groups, respectively.[118]) The singular peak that is obtained for cubane is more intense than the leading x-ray absorption features for adamantane or twistane, suggesting a pair of peaks whose splitting is smaller than what is observed experimentally.

E. Electronic structure of organotitanium complexes

Solomon and co-workers have investigated pre-edge features of the organotitanium complexes $TiCl_4$, $TiCpCl_3$, and $TiCp_2Cl_2$,[34] where Cp = $(C_5H_5)^-$ is the cyclopentadiene anion. (These are models of the anti-tumor agent titanocene dichloride.[119]) As shown in Fig. 6(a), the titanium K-edge appears at 4980 eV, although it is the pre-edge that is of primary interest as it contains information about metal–ligand hybridization. A $1s \rightarrow 3d$ pre-edge transition is obtained at 4976 eV using CAM-B3LYP/CIS, and the spectrum in Fig. 6(a) is shifted by about 7 eV to match the experimental peak at 4969 eV. This transition is electric-dipole forbidden but quadrupole-allowed and appears primarily due to mixing of Ti($4p$) and Ti($3d$) orbitals.[34] The pre-edge feature is most intense for $TiCl_4$, with the intensity diminishing in $TiCp_3Cl$ and $TiCp_2Cl_2$.

At the chlorine K-edge, there is also an intense pre-edge feature for all three complexes [Fig. 6(b)]. CAM-B3LYP/CIS spectra need a 6.7 eV shift to match the experimental peak at 2820 eV. It is most intense for $TiCl_4$ and decreases in intensity with the addition of each subsequent Cp ligand, a trend that is reproduced by the CAM-B3LYP/CIS calculations and arises due to decreased covalency of the remaining Ti–Cl bonds as Cl ligands are replaced by Cp ligands.[34]

For $TiCpCl_3$ and $TiCp_2Cl_2$, there are peak splittings in the pre-edge features that were reported experimentally, arising from the splitting of the Ti($3d$) e and t_2 orbitals. Peak assignments for these pre-edge features have been discussed at length;[34] for the present purposes, it suffices to note that these features are reproduced in the CAM-B3LYP/CIS spectra. Addition of Cp ligands results in strong π–donor interactions between the Cp ligand and the metal d_{xz} and d_{yz} orbitals, resulting in the splitting. This is more apparent at the chlorine K-edge due to the reduction of Cl($3p$) contributions to the Ti($3d$) orbitals when Cl is replaced by Cp. With the increase in the number of Cp ligands, the splitting changes. Higher-energy d-orbitals have a more significant contribution from the Cp ligands; hence, with an increased number of Cp ligands, the intensity of the splitting is reversed. Experimentally, this happens at both the titanium and chlorine K-edges, although in the simulated spectra the effect is more prominent at the chlorine K-edge.

The advantage of accurate spectra is especially apparent in this case, as we obtain absolute excitation energies (without shifting) that differ by only a few eV from the experimental spectra at energies of several thousand eV. As such, there is no need for large-scale shifting (by tens or even hundreds of eV) that is common in TD-DFT calculations for metal K-edges, as documented in Table II for several $3d$ metal atoms. In the present case, TD-CAM-B3LYP/def2-TZVPD spectra at the Ti K-edge must be shifted by a further 76 eV in order to match experiment (Fig. S2). For XANES at the Cl K-edge, the TD-CAM-B3LYP/def2-TZVPD spectra must be shifted by an additional 56 eV, relative to CAM-B3LYP/CIS/def2-TZVPD, in order to coincide with experiment (Fig. S3). In complex systems with multiple overlapping edges, the need for large shifts can render it difficult to understand the spectra. In the case of titania, for example, the Ti L_1-edge overlaps with the oxygen K-edge.[26]

F. X-ray emission spectra

Figure 7 shows experimental XES spectra of H_2S[120] and CH_3Cl[121] at the sulfur and chlorine K-edges, juxtaposed with

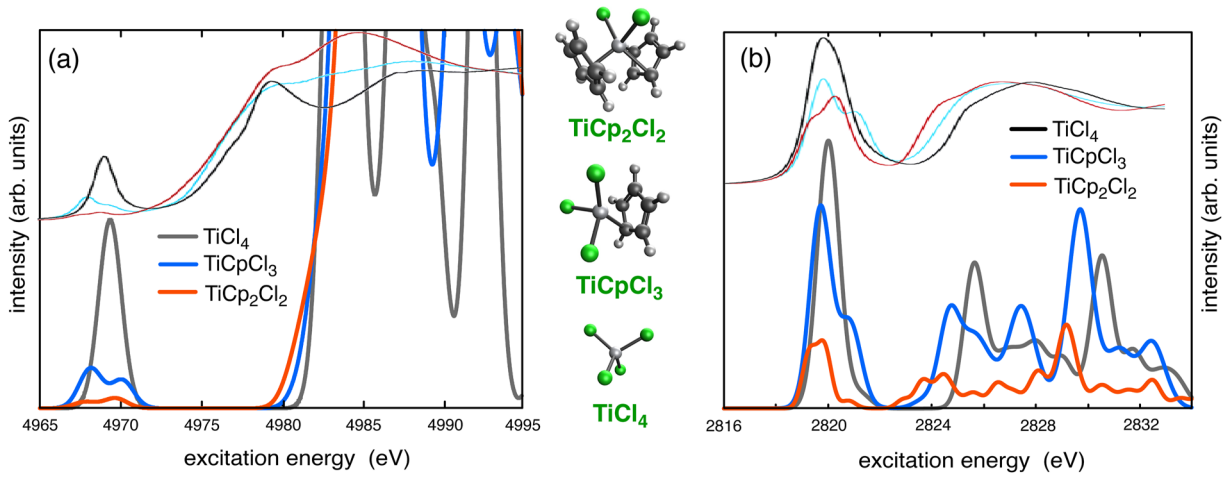

FIG. 6. Absorption spectra of $TiCl_4$, $TiCpCl_3$, and $TiCp_2Cl_2$ at (a) the titanium K-edge and (b) the chlorine K-edge. Calculations were performed at the CAM-B3LYP/CIS level, using 200 states for the titanium K-edge and 300 states for chlorine, broadened by Gaussians of width 0.70 eV (Ti) and 0.17 eV (Cl) and shifted by 7.0 eV (Ti) and 6.7 eV (Cl). Pre-edge features were compared to solution-phase experimental spectra (at the top) that are reproduced from Ref. 34.

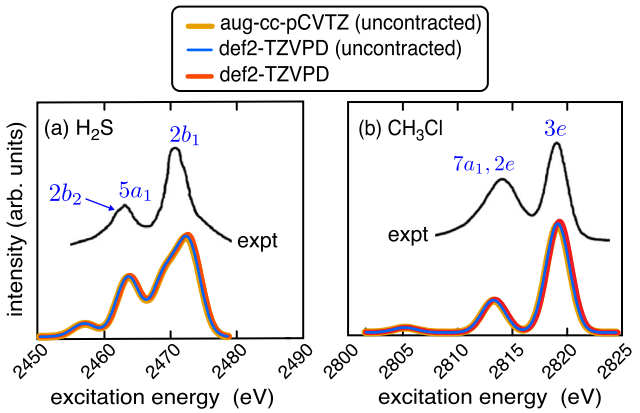

FIG. 7. Simulated XES for (a) H_2S and (b) CH_3Cl, computed using CAM-B3LYP/CIS and shifted by 27 and 28 eV, respectively, and compared to experimental spectra from Refs. 120 and 121. Peak assignments are from the experimental papers and correspond to emission from the indicated orbital into the $1a_1$ MO. Simulated spectra are shown using several different basis sets, two of which are uncontracted. These spectra include 200 states, each with a Gaussian broadening of 0.6 eV.

simulated CAM-B3LYP/CIS spectra. (The calculations use the procedure that was outlined in Sec. II D, based on the maximum overlap method.[76]) The simulated spectra are in reasonable agreement with experiment and require smaller shifts as compared to other TD-DFT approaches.[73,122] This means that the accuracy is much improved relative to TD-B3LYP or TD-CAM-B3LYP, which we attribute to the additional Hartree–Fock exchange that is incorporated either at short range (in the case of the SRC1 functionals, which were used to parameterize $\Delta\varepsilon$) or else added directly to the CIS matrix elements (for CAM-B3LYP/CIS). However, the shift that is needed to match experiment is about 28 eV for CH_3Cl, which is larger than what was required for chlorine K-edge absorption in CH_3Cl (see Table II) and also larger than the shifts required to match the experiment for (cyclopentadienyl)titanium compounds (Sec. IV E).

For XANES, previous basis-set testing suggests that the demands of core-level absorption spectroscopy are not much different from those of valence TD-DFT calculations,[26] meaning that double-ζ basis sets are often sufficient.[10] This contrasts with the situation for correlated wave function models, where an improved treatment of the core functions is imperative,[123,124] and there has been some suggestion that basis-set effects are more significant in TD-DFT calculations of XES spectra.[73,125] Our results suggest this is not the case, however.

An improved description of the core can be obtained by uncontracting the core functions in standard Gaussian basis sets[26,82,126] or by using basis sets containing core polarization functions such as those in the cc-pCVXZ sequence.[117] Spectra obtained using uncontracted versions of def2-TZVPD and aug-cc-pCVTZ are virtually identical (Fig. 7). Furthermore, the difference between normal (contracted) def2-TZVPD and uncontracted aug-cc-pCVTZ is only about 1 eV for H_2S and 0.5 eV for CH_3Cl. As such, the net effect of uncontracted basis sets for H_2S is that the shift required to match the experiment is reduced from 28 eV (def2-TZVPD) to 27 eV (uncontracted aug-cc-pCVTZ or uncontracted def2-TZVPD). For CH_3Cl, both basis sets afford essentially identical spectra that are shifted from the experiment by ~28 eV. Both of these results are an improvement over the corresponding TD-CAM-B3LYP/def2-TZVPD calculations, which require shifts of 45 eV (CH_3Cl, Fig. S4) and 41 eV (H_2S, Fig. S5) in order to match experiment. Still, the shifts required for XES using CAM-B3LYP/CIS are larger than those required for XANES, and basis-set effects do not explain this discrepancy.

G. L-edge spectra

Inaccuracies in XES as compared to XANES led us to investigate the nature of our DFT/CIS parameterization, specifically the shifting of the core orbital energies, and why this procedure does not work as well for XES. One observation is that the core hole generated in the non-*Aufbau* XES reference state, which is an empty

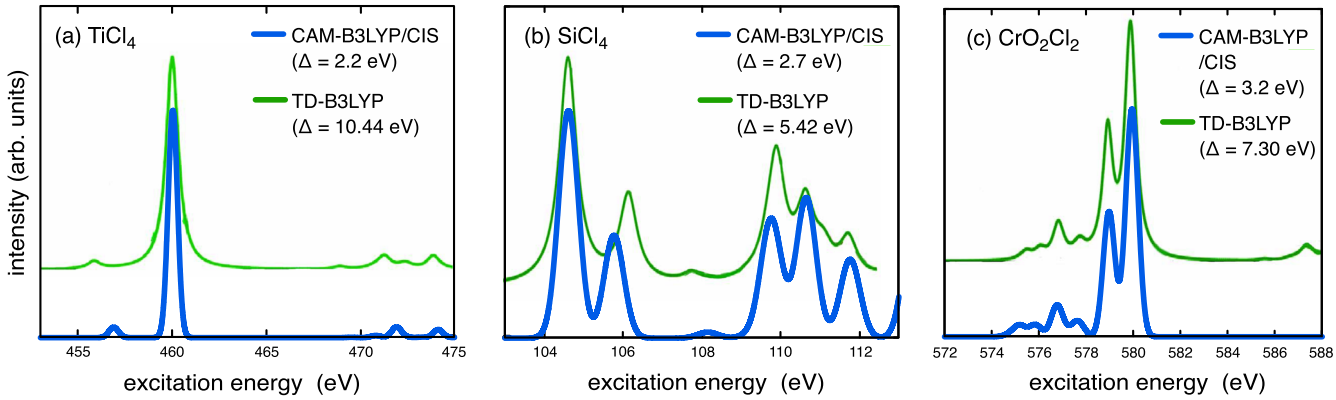

FIG. 8. Simulated L-edge XANES for (a) $TiCl_4$, (b) $SiCl_4$, and (c) CrO_2Cl_2, with shifts (Δ) as indicated. The CAM-B3LYP/CIS spectra include 400 states, broadened using a 0.2 eV Gaussian function. The TD-B3LYP spectra were broadened using a Lorentzian of width 0.5 eV and are reproduced from Ref. 127. All spectra are computed without spin–orbit coupling effects using the def2-TZVPD basis set.

unrestricted orbital with β spin, is lower in energy than the corresponding α-spin 1*s* occupied orbital by about 0.5 E_h or ~10 eV. This could adversely interact with the parameterization of $\Delta\varepsilon$, which is based on restricted (closed-shell) orbital energies, such that orbital relaxation effects on the core hole are not built into the parameterization, although they are included in the XES procedure that is outlined in Sec. II D. We considered that this might imply that the DFT/CIS parameterization is suitable only to describe excitations out of 1*s* orbitals, meaning elemental K-edge spectra, and might fail to account for the differential SIE and orbital relaxation effects in the case of L- and M-edge spectra.

To investigate this, we computed L-edge XANES of three molecules considered previously at the TD-B3LYP level,[127] with simulated spectra shown in Fig. 8. Spin–orbit couplings are neglected in both the CAM-B3LYP/CIS and TD-B3LYP spectra, as our primary objective is to observe the scalar shifts required for either method, which were optimized for TD-B3LYP in Ref. 127 in order to put the spin-orbit-free L-edge feature between the experimental L_2- and L_3-edge peaks. Essential features of the spin-orbit-free L-edge spectra are quite similar at the two levels of theory, but the requisite shifts are considerably smaller in the case of CAM-B3LYP/CIS; see Fig. 8. Indeed, for CAM-B3LYP/CIS, the shifts required for L-edge spectroscopy are similar in magnitude to those required for K-edge XANES, which suggests that the method works about equally well for both K- and L-edge XANES but less well for XES, where the reference state is open-shell. The effects of differential (core vs valence) SIE and orbital relaxation appear to be balanced by the correction $\Delta\varepsilon$, but only for closed-shell reference states. This warrants further investigation.

V. CONCLUSIONS

The present work reports a parameterization of DFT/CIS based on the CAM-B3LYP functional for elements through the 3*d* transition metals. Given a suitable parameterization, this approach improves considerably upon most TD-DFT calculations (including TD-CAM-B3LYP) for K- and L-edge XANES and K-edge XES. The DFT/CIS formalism adds extra Hartree–Fock exchange but omits any XC kernel in the matrix elements of the excited-state eigenvalue problem. (The effect of these matrix elements in many XANES applications is only ~0.5 eV.[128]) The cost of DFT/CIS is identical to that of CIS, which can be formulated in a very efficient, integral-direct manner.[22–26] Within the CVS approximation that is used for core-level spectroscopy, the cost remains modest even when hundreds of excited states are required.[26]

The new CAM-B3LYP/CIS method dramatically reduces the need for large shifts that are required in most TD-DFT calculations of core-level spectra, although more so for XAS than for XES. Comparison to DFT/MRCI results and Grimme's original B3LYP-based parameterization of DFT/CIS suggests that parameterized adjustments to core-level Kohn–Sham eigenvalues are more important than electron correlation effects *per se*. The new approach reproduces experimental pre-edge and near-edge features for a variety of chemical systems, and only modest shifts are required to match experimental features in absolute terms. This should aid in the assignment of complex spectra with overlapping features. At the same time, CAM-B3LYP/CIS remains useful for valence spectroscopy. The addition of spin–orbit couplings is currently underway, which will facilitate direct comparison to experiment for L- and M-edge spectra.

SUPPLEMENTARY MATERIAL

The supplementary material includes coordinates for all test systems used here and a specification of the VTZ+ basis set.

ACKNOWLEDGMENTS

Work by A.M. was supported by the donors of the ACS Petroleum Research Fund under Grant No. 62041-ND6. J.M.H. acknowledges additional support from the National Science Foundation under Grant No. CHE-1955282. Calculations were performed at the Ohio Supercomputer Center.[129]

AUTHOR DECLARATIONS

Conflict of Interest

J.M.H. is part owner of Q-Chem and serves on its board of directors.

Author Contributions

Aniket Mandal: Conceptualization (contributing); Data curation (lead); Formal analysis (lead); Investigation (lead); Methodology (lead); Software (lead); Validation (lead); Visualization (lead); Writing – original draft (lead); Writing – review and editing (equal). **Eric J. Berquist**: Software (contributing); Supervision (contributing). **John M. Herbert**: Conceptualization (lead); Formal analysis (contributing); Funding acquisition (lead); Methodology (contributing); Project administration (lead); Supervision (lead); Visualization (contributing); Writing – review and editing (equal).

DATA AVAILABILITY

The data that support the findings of this study are available from the corresponding author upon reasonable request.

REFERENCES

[1] J. C. Sancho-García and C. Adamo, "Double-hybrid density functionals: Merging wavefunction and density approaches to get the best of both worlds," Phys. Chem. Chem. Phys. **15**, 14581–14594 (2013).
[2] X. Zhang and J. M. Herbert, "Spin-flip, tensor equation-of-motion configuration interaction with a density-functional correction: A spin-complete method for exploring excited-state potential energy surfaces," J. Chem. Phys. **143**, 234107 (2015).
[3] S. Ghosh, P. Verma, C. J. Cramer, L. Gagliardi, and D. G. Truhlar, "Combining wave function methods with density functional theory for excited states," Chem. Rev. **118**, 7249–7292 (2018).
[4] C. M. Marian, A. Heil, and M. Kleinschmidt, "The DFT/MRCI method," Wiley Interdiscip. Rev. Comput. Mol. Sci. **9**, e1394 (2018); Erratum **9**, e1437 (2019).
[5] E. D. Hedegård, J. Toulouse, and H. J. A. Jensen, "Multiconfigurational short-range density-functional theory for open-shell systems," J. Chem. Phys. **148**, 214103 (2018).

[6]C. Kalai, B. Mussard, and J. Toulouse, "Range-separated double-hybrid density-functional theory with coupled-cluster and random-phase approximations," J. Chem. Phys. **151**, 074102 (2019).
[7]D. Casanova, "Restricted active space configuration interaction methods for strong correlation: Recent developments," WIREs Compu. Mol. Sci. **12**, e1561 (2021).
[8]J. M. Herbert and A. Mandal, "Spin-flip TDDFT for photochemistry," in *Time-Dependent Density Functional Theory: Nonadiabatic Molecular Dynamics*, edited by C. Zhu (Jenny Stanford, 2023), Chap. 10, pp. 361–404.
[9]S. Grimme, "Density functional calculations with configuration interaction for the excited states of molecules," Chem. Phys. Lett. **259**, 128–137 (1996).
[10]J. M. Herbert, "Density-functional theory for electronic excited states," in *Theoretical and Computational Photochemistry: Fundamentals, Methods, Applications and Synergy with Experimental Approaches*, edited by C. García-Iriepa and M. Marazzi (Elsevier, Amsterdam, 2023), Chap. 3, pp. 69–118.
[11]S. Grimme and M. Waletzke, "A combination of Kohn–Sham density functional theory and multi-reference configuration interaction methods," J. Chem. Phys. **111**, 5645–5655 (1999).
[12]I. Lyskov, M. Kleinschmidt, and C. M. Marian, "Redesign of the DFT/MRCI Hamiltonian," J. Chem. Phys. **144**, 034104 (2016).
[13]A. Heil and C. M. Marian, "DFT/MRCI Hamiltonian for odd and even numbers of electrons," J. Chem. Phys. **147**, 194104 (2017); Erratum **150**, 219902 (2019).
[14]V. Jovanović, I. Lyskov, M. Kleinschmidt, and C. M. Marian, "On the performance of DFT/MRCI-R and MR-MP2 in spin–orbit coupling calculations on diatomics and polyatomic organic molecules," Mol. Phys. **115**, 109–137 (2017).
[15]A. Heil, M. Kleinschmidt, and C. M. Marian, "On the performance of DFT/MRCI Hamiltonians for electronic excitations in transition metal complexes: The role of the damping function," J. Chem. Phys. **149**, 164106 (2018); Erratum **150**, 219903 (2019).
[16]M. Bracker, C. M. Marian, and M. Kleinschmidt, "Internal conversion of singlet and triplet states employing numerical DFT/MRCI derivative couplings: Implementation, tests, and application to xanthone," J. Chem. Phys. **155**, 014102 (2021).
[17]D. R. Dombrowski, T. Schulz, M. Kleinschmidt, and C. M. Marian, "R2022: A DFT/MRCI ansatz with improved performance for double excitations," J. Phys. Chem. A **127**, 2011–2025 (2023).
[18]T. Schulz, S. Hédé, O. Weingart, and C. M. Marian, "Multiexcitonic and optically bright states in subunits of pentacene crystals: A hybrid DFT/MRCI and molecular mechanics study," J. Chem. Phys. **160**, 144114 (2024).
[19]I. Seidu, S. P. Neville, M. Kleinschmidt, A. Heil, C. M. Marian, and M. S. Schuurman, "The simulation of x-ray absorption spectra from ground and excited electronic states using core-valence separated DFT/MRCI," J. Chem. Phys. **151**, 144104 (2019).
[20]S. P. Neville and M. S. Schuurman, "Removing the deadwood from DFT/MRCI wave functions: The p-DFT/MRCI method," J. Chem. Theory Comput. **17**, 7657–7665 (2021).
[21]S. P. Neville and M. S. Schuurman, "A perturbative approximation to DFT/MRCI: DFT/MRCI(2)," J. Chem. Phys. **157**, 164103 (2022).
[22]H. Weiss, R. Ahlrichs, and M. Häser, "A direct algorithm for self-consistent-field linear response theory and application to C_{60}: Excitation energies, oscillator strengths, and frequency-dependent polarizabilities," J. Chem. Phys. **99**, 1262–1270 (1993).
[23]D. R. Maurice, "Single electron theories of excited states," Ph.D. thesis, University of California, Berkeley, CA, 1998.
[24]F. Furche and D. Rappoport, "Density functional methods for excited states: Equilibrium structure and electronic spectra," in *Computational Photochemistry*, *Theoretical and Computational Chemistry Vol. 16*, edited by M. Olivucci (Elsevier, Amsterdam, 2005), Chap. 3, pp. 93–128.
[25]A. F. Morrison, E. Epifanovsky, and J. M. Herbert, "Double-buffered, heterogeneous CPU + GPU integral digestion algorithm for single-excitation calculations involving a large number of excited states," J. Comput. Chem. **39**, 2173–2182 (2018).
[26]J. M. Herbert, Y. Zhu, B. Alam, and A. K. Kumar, "Time-dependent density functional theory for x-ray absorption spectra: Comparing the real-time approach to linear response," J. Chem. Theory Comput. **19**, 6745–6760 (2023).
[27]D. Maurice and M. Head-Gordon, "Configuration interaction with single substitutions for excited states of open-shell molecules," Int. J. Quantum Chem. **56**, 361–370 (1995).
[28]M. Roemelt and F. Neese, "Excited states of large open-shell molecules: An efficient, general, and spin-adapted approach based on a restricted open-shell ground state wave function," J. Phys. Chem. A **117**, 3069–3083 (2013).
[29]M. Roemelt, D. Maganas, S. DeBeer, and F. Neese, "A combined DFT and restricted open-shell configuration interaction method including spin-orbit coupling: Application to transition metal L-edge x-ray absorption spectroscopy," J. Chem. Phys. **138**, 204101 (2013).
[30]J. Stöhr, *NEXAFS Spectroscopy*, 1st ed., *Springer Series in Surface Sciences Vol. 25* (Springer-Verlag, Berlin, 1992).
[31]T. E. Westre, P. Kennepohl, J. G. DeWitt, B. Hedman, K. O. Hodgson, and E. I. Solomon, "A multiplet analysis of Fe K-Edge 1s → 3d pre-edge features of iron complexes," J. Am. Chem. Soc. **119**, 6297–6314 (1997).
[32]J. L. DuBois, P. Mukherjee, A. M. Collier, J. M. Mayer, E. I. Solomon, B. Hedman, T. D. P. Stack, and K. O. Hodgson, "Cu K-edge XAS study of the $[Cu_2(\mu\text{-}O)_2]$ core: Direct experimental evidence for the presence of Cu(III)," J. Am. Chem. Soc. **119**, 8578–8579 (1997).
[33]F. Farges, G. E. Brown, Jr., and J. J. Rehr, "Ti *K*-edge XANES studies of Ti coordination and disorder in oxide compounds: Comparison between theory and experiment," Phys. Rev. B **56**, 1809–1819 (1997).
[34]S. DeBeer George, P. Brant, and E. I. Solomon, "Metal and ligand K-edge XAS of organotitanium complexes: Metal 4p and 3d contributions to pre-edge intensity and their contributions to bonding," J. Am. Chem. Soc. **127**, 667–674 (2005).
[35]S. DeBeer George, T. Petrenko, and F. Neese, "Prediction of iron K-edge absorption spectra using time-dependent density functional theory," J. Phys. Chem. A **112**, 12936–12943 (2008).
[36]A. Nakata, Y. Imamura, T. Otsuka, and H. Nakai, "Time-dependent density functional theory calculations for core-excited states: Assessment of standard exchange-correlation functionals and development of a novel hybrid functional," J. Chem. Phys. **124**, 094105 (2006).
[37]A. Nakata, Y. Imamura, and H. Nakai, "Hybrid exchange-correlation functional for core, valence, and Rydberg excitations: Core-valence-Rydberg B3LYP," J. Chem. Phys. **125**, 064109 (2006).
[38]N. A. Besley, M. J. G. Peach, and D. J. Tozer, "Time-dependent density functional theory calculations of near-edge x-ray absorption fine structure with short-range corrected functionals," Phys. Chem. Chem. Phys. **11**, 10350–10358 (2009).
[39]N. A. Besley and F. A. Asmuruf, "Time-dependent density functional theory calculations of the spectroscopy of core electrons," Phys. Chem. Chem. Phys. **12**, 12024–12039 (2010).
[40]A. Nakata, Y. Imamura, and H. Nakai, "Extension of the core-valence-Rydberg B3LYP functional to core-excited-state calculations of third-row atoms," J. Chem. Theory Comput. **3**, 1295–1305 (2007).
[41]M. Roemelt, M. A. Beckwith, C. Duboc, M.-N. Collomb, F. Neese, and S. DeBeer, "Manganese K-edge X-ray absorption spectroscopy as a probe of the metal–ligand interactions in coordination compounds," Inorg. Chem. **51**, 680–687 (2012).
[42]T. Fransson, I. E. Brumboiu, M. L. Vidal, P. Norman, S. Coriani, and A. Dreuw, "Xaboom: An x-ray absorption benchmark of organic molecules based on carbon, nitrogen, and oxygen 1s → π^* transitions," J. Chem. Theory Comput. **17**, 1618–1637 (2021).
[43]N. A. Besley, "Modeling of the spectroscopy of core electrons with density functional theory," WIREs Compu. Mol. Sci. **11**, e1527 (2021).
[44]A. Szabo and N. S. Ostlund, *Modern Quantum Chemistry* (Dover Publications, 1996).
[45]Our notation for the Coulomb (J_{ia}) and exchange (K_{ia}) integrals is opposite to that used in Grimme's original work[9] but is consistent with standard quantum chemistry notation.[44]
[46]A. Savin, C. J. Umrigar, and X. Gonze, "Relationship of Kohn–Sham eigenvalues to excitation energies," Chem. Phys. Lett. **288**, 391–395 (1998).
[47]M. Petersilka, E. K. U. Gross, and K. Burke, "Excitation energies from time-dependent density functional theory using exact and approximate potentials," Int. J. Quantum Chem. **80**, 534–554 (2000).

[48]E. J. Baerends, O. V. Gritsenko, and R. van Meer, "The Kohn–Sham gap, the fundamental gap and the optical gap: The physical meaning of occupied and virtual Kohn–Sham orbital energies," Phys. Chem. Chem. Phys. **15**, 16408–16425 (2013).
[49]J. M. Herbert, "Visualizing and characterizing excited states from time-dependent density functional theory," Phys. Chem. Chem. Phys. **26**, 3755–3794 (2024).
[50]J. M. Herbert, "The quantum chemistry of loosely-bound electrons," in *Reviews in Computational Chemistry*, edited by A. L. Parill and K. Lipkowitz (Wiley-VCH, Hoboken, 2015), Vol. 28, Chap. 8, pp. 391–517.
[51]A. D. Becke, "Density-functional thermochemistry. III. The role of exact exchange," J. Chem. Phys. **98**, 5648–5652 (1993).
[52]C. Lee, W. Yang, and R. G. Parr, "Development of the Colle-Salvetti correlation-energy formula into a functional of the electron density," Phys. Rev. B **37**, 785–789 (1988).
[53]M. A. Rohrdanz and J. M. Herbert, "Simultaneous benchmarking of ground- and excited-state properties with long-range-corrected density functional theory," J. Chem. Phys. **129**, 034107 (2008).
[54]B. Alam, A. F. Morrison, and J. M. Herbert, "Charge separation and charge transfer in the low-lying excited states of pentacene," J. Phys. Chem. C **124**, 24653–24666 (2020).
[55]T. Yanai, D. P. Tew, and N. C. Handy, "A new hybrid exchange-correlation functional using the Coulomb-attenuating method (CAM-B3LYP)," Chem. Phys. Lett. **393**, 51–57 (2004).
[56]F. Weigend and R. Ahlrichs, "Balanced basis sets of split valence, triple zeta valence and quadruple zeta valence quality for H to Rn: Design and assessment of accuracy," Phys. Chem. Chem. Phys. **7**, 3297–3305 (2005).
[57]D. Rappoport and F. Furche, "Property-optimized Gaussian basis sets for molecular response calculations," J. Chem. Phys. **133**, 134105 (2010).
[58]P.-F. Loos, A. Scemama, A. Blondel, Y. Garniron, M. Caffarel, and D. Jacquemin, "A mountaineering strategy to excited states: Highly accurate reference energies and benchmarks," J. Chem. Theory Comput. **14**, 4360–4379 (2018).
[59]N. A. Besley, "Density functional theory based methods for the calculation of x-ray spectroscopy," Acc. Chem. Res. **53**, 1306–1315 (2020).
[60]D. P. Chong, O. V. Gritsenko, and E. J. Baerends, "Interpretation of the Kohn–Sham orbital energies as approximate vertical ionization potentials," J. Chem. Phys. **116**, 1760–1772 (2002).
[61]P. Verma and R. J. Bartlett, "Increasing the applicability of density functional theory. IV. Consequences of ionization-potential improved exchange-correlation potentials," J. Chem. Phys. **140**, 18A534 (2014).
[62]K. Carter-Fenk, L. A. Cunha, J. E. Arias-Martinez, and M. Head-Gordon, "Electron-affinity time-dependent density functional theory: Formalism and applications to core-excited states," J. Phys. Chem. Lett. **13**, 9664–9672 (2022).
[63]R. M. Richard and J. M. Herbert, "Time-dependent density-functional description of the ^1L_a state in polycyclic aromatic hydrocarbons: Charge-transfer character in disguise?," J. Chem. Theory Comput. **7**, 1296–1306 (2011).
[64]S. Jana and J. M. Herbert, "Slater transition methods for core-level electron binding energies," J. Chem. Phys. **158**, 094111 (2023).
[65]S. Jana and J. M. Herbert, "Fractional-electron and transition-potential methods for core-to-valence excitation energies using density functional theory," J. Chem. Theory Comput. **19**, 4100–4113 (2023); Erratum **19**, 7432–7433 (2023).
[66]M. A. Rohrdanz, K. M. Martins, and J. M. Herbert, "A long-range-corrected density functional that performs well for both ground-state properties and time-dependent density functional theory excitation energies, including charge-transfer excited states," J. Chem. Phys. **130**, 054112 (2009).
[67]J.-W. Song, M. A. Watson, A. Nakata, and K. Hirao, "Core-excitation energy calculations with a long-range corrected hybrid exchange-correlation functional including a short-range Gaussian attenuation (LCgau-BOP)," J. Chem. Phys. **129**, 184113 (2008).
[68]N. A. Besley, "Equation of motion coupled cluster theory calculations of the x-ray emission spectroscopy of water," Chem. Phys. Lett. **542**, 42–46 (2012).
[69]O. V. Ershova and N. A. Besley, "Theoretical calculations of the excited state potential energy surfaces of nitric oxide," Chem. Phys. Lett. **513**, 179–183 (2011).
[70]X. Zheng and L. Cheng, "Performance of delta-coupled-cluster methods for calculations of core-ionization energies of first-row elements," J. Chem. Theory Comput. **15**, 4945–4955 (2019).
[71]M. P. Coons and J. M. Herbert, "Quantum chemistry in arbitrary dielectric environments: Theory and implementation of nonequilibrium Poisson boundary conditions and application to compute vertical ionization energies at the air/water interface," J. Chem. Phys. **148**, 222834 (2018); Erratum **151**, 189901 (2019).
[72]I. E. Brumboiu and T. Fransson, "Core–hole delocalization for modeling x-ray spectroscopies: A cautionary tale," J. Chem. Phys. **156**, 214109 (2022).
[73]J. D. Wadey and N. A. Besley, "Quantum chemical calculations of x-ray emission spectroscopy," J. Chem. Theory Comput. **10**, 4557–4564 (2014).
[74]Y. Zhang, S. Mukamel, M. Khalil, and N. Govind, "Simulating valence-to-core x-ray emission spectroscopy of transition metal complexes with time-dependent density functional theory," J. Chem. Theory Comput. **11**, 5804–5809 (2015).
[75]D. R. Nascimento and N. Govind, "Computational approaches for XANES, VtC-XES, and RIXS using linear-response time-dependent density functional theory based methods," Phys. Chem. Chem. Phys. **24**, 14680–14691 (2022).
[76]A. T. B. Gilbert, N. A. Besley, and P. M. W. Gill, "Self-consistent field calculations of excited states using the maximum overlap method (MOM)," J. Phys. Chem. A **112**, 13164–13171 (2008).
[77]D. Hait and M. Head-Gordon, "Excited state orbital optimization via minimizing the square of the gradient: General approach and application to singly and doubly excited states via density functional theory," J. Chem. Theory Comput. **16**, 1699–1710 (2020).
[78]K. Carter-Fenk and J. M. Herbert, "State-targeted energy projection: A simple and robust approach to orbital relaxation of non-aufbau self-consistent field solutions," J. Chem. Theory Comput. **16**, 5067–5082 (2020).
[79]By default, the Q-Chem program uses two SCF cycles (Roothaan steps) to ensure that [**F**, **P**] = **0** for any user-defined set of guess orbitals, so this behavior shoud be deactivated for XES calculations.
[80]E. Epifanovsky, A. T. B. Gilbert, X. Feng, J. Lee, Y. Mao, N. Mardirossian, P. Pokhilko, A. F. White, M. P. Coons, A. L. Dempwolff, Z. Gan, D. Hait, P. R. Horn, L. D. Jacobson, I. Kaliman, J. Kussmann, A. W. Lange, K. U. Lao, D. S. Levine, J. Liu, S. C. McKenzie, A. F. Morrison, K. D. Nanda, F. Plasser, D. R. Rehn, M. L. Vidal, Z.-Q. You, Y. Zhu, B. Alam, B. J. Albrecht, A. Aldossary, E. Alguire, J. H. Andersen, V. Athavale, D. Barton, K. Begam, A. Behn, N. Bellonzi, Y. A. Bernard, E. J. Berquist, H. G. A. Burton, A. Carreras, K. Carter-Fenk, R. Chakraborty, A. D. Chien, K. D. Closser, V. Cofer-Shabica, S. Dasgupta, M. de Wergifosse, J. Deng, M. Diedenhofen, H. Do, S. Ehlert, P.-T. Fang, S. Fatehi, Q. Feng, T. Friedhoff, J. Gayvert, Q. Ge, G. Gidofalvi, M. Goldey, J. Gomes, C. E. González-Espinoza, S. Gulania, A. O. Gunina, M. W. D. Hanson-Heine, P. H. P. Harbach, A. Hauser, M. F. Herbst, M. Hernández Vera, M. Hodecker, Z. C. Holden, S. Houck, X. Huang, K. Hui, B. C. Huynh, M. Ivanov, A. Jász, H. Ji, H. Jiang, B. Kaduk, S. Kähler, K. Khistyaev, J. Kim, G. Kis, P. Klunzinger, Z. Koczor-Benda, J. H. Koh, D. Kosenkov, L. Koulias, T. Kowalczyk, C. M. Krauter, K. Kue, A. Kunitsa, T. Kus, I. Ladjánszki, A. Landau, K. V. Lawler, D. Lefrancois, S. Lehtola, R. R. Li, Y.-P. Li, J. Liang, M. Liebenthal, H.-H. Lin, Y.-S. Lin, F. Liu, K.-Y. Liu, M. Loipersberger, A. Luenser, A. Manjanath, P. Manohar, E. Mansoor, S. F. Manzer, S.-P. Mao, A. V. Marenich, T. Markovich, S. Mason, S. A. Maurer, P. F. McLaughlin, M. F. S. J. Menger, J.-M. Mewes, S. A. Mewes, P. Morgante, J. W. Mullinax, K. J. Oosterbaan, G. Paran, A. C. Paul, S. K. Paul, F. Pavošević, Z. Pei, S. Prager, E. I. Proynov, A. Rák, E. Ramos-Cordoba, B. Rana, A. E. Rask, A. Rettig, R. M. Richard, F. Rob, E. Rossomme, T. Scheele, M. Scheurer, M. Schneider, N. Sergueev, S. M. Sharada, W. Skomorowski, D. W. Small, C. J. Stein, Y.-C. Su, E. J. Sundstrom, Z. Tao, J. Thirman, G. J. Tornai, T. Tsuchimochi, N. M. Tubman, S. P. Veccham, O. Vydrov, J. Wenzel, J. Witte, A. Yamada, K. Yao, S. Yeganeh, S. R. Yost, A. Zech, I. Y. Zhang, X. Zhang, Y. Zhang, D. Zuev, A. Aspuru-Guzik, A. T. Bell, N. A. Besley, K. B. Bravaya, B. R. Brooks, D. Casanova, J.-D. Chai, S. Coriani, C. J. Cramer, G. Cserey, A. E. DePrince III, R. A. DiStasio, Jr., A. Dreuw, B. D. Dunietz, T. R. Furlani, W. A. Goddard III, S. Hammes-Schiffer, T. Head-Gordon, W. J. Hehre, C.-P. Hsu, T.-C. Jagau, Y. Jung, A. Klamt, J. Kong, D. S. Lambrecht, W. Liang, N. J. Mayhall, C. W. McCurdy, J. B. Neaton, C. Ochsenfeld, J. A. Parkhill, R. Peverati, V. A. Rassolov, Y. Shao, L. V. Slipchenko, T. Stauch, R. P. Steele, J. E. Subotnik, A. J. W. Thom, A. Tkatchenko, D. G. Truhlar, T. Van Voorhis, T. A. Wesolowski, K. B. Whaley, H. L. Woodcock III, P. M. Zimmerman, S. Faraji, P. M. W. Gill, M. Head-Gordon, J. M. Herbert, and A. I. Krylov, "Software for the frontiers of quantum chemistry: An overview of developments in the Q-Chem 5 package," J. Chem. Phys. **155**, 084801 (2021).
[81]M. F. Herbst and T. Fransson, "Quantifying the error of the core–valence separation approximation," J. Chem. Phys. **153**, 054114 (2020).

[82]N. A. Besley, A. T. B. Gilbert, and P. M. W. Gill, "Self-consistent-field calculations of core excited states," J. Chem. Phys. **130**, 124308 (2009).
[83]A. A. E. Fouda and N. A. Besley, "Improving the predictive quality of time-dependent density functional theory calculations of the X-ray emission spectroscopy of organic molecules," J. Comput. Chem. **41**, 1081–1090 (2020).
[84]M. Reiher, "Douglas–Kroll–Hess theory: A relativistic electrons-only theory for chemistry," Theor. Chem. Acc. **116**, 241–252 (2006).
[85]T. Nakajima and K. Hirao, "The Douglas–Kroll–Hess approach," Chem. Rev. **112**, 385–402 (2012).
[86]M. Reiher and A. Wolf, *Relativistic Quantum Chemistry: The Fundamental Theory of Molecular Science*, 2nd ed. (Wiley-VCH, 2015).
[87]W. A. de Jong, R. J. Harrison, and D. A. Dixon, "Parallel Douglas–Kroll energy and gradients in NWChem: Estimating scalar relativistic effects using Douglas–Kroll contracted basis sets," J. Chem. Phys. **114**, 48–53 (2001).
[88]E. Aprà, E. J. Bylaska, W. A. de Jong, N. Govind, K. Kowalski, T. P. Straatsma, M. Valiev, H. J. J. van Dam, Y. Alexeev, J. Anchell, V. Anisimov, F. W. Aquino, R. Atta-Fynn, J. Autschbach, N. P. Bauman, J. C. Becca, D. E. Bernholdt, K. Bhaskaran-Nair, S. Bogatko, P. Borowski, J. Boschen, J. Brabec, A. Bruner, E. Cauët, Y. Chen, G. N. Chuev, C. J. Cramer, J. Daily, M. J. O. Deegan, T. H. Dunning, M. Dupuis, K. G. Dyall, G. I. Fann, S. A. Fischer, A. Fonari, H. Früchtl, L. Gagliardi, J. Garza, N. Gawande, S. Ghosh, K. Glaesemann, A. W. Götz, J. Hammond, V. Helms, E. D. Hermes, K. Hirao, S. Hirata, M. Jacquelin, L. Jensen, B. G. Johnson, H. Jónsson, R. A. Kendall, M. Klemm, R. Kobayashi, V. Konkov, S. Krishnamoorthy, M. Krishnan, Z. Lin, R. D. Lins, R. J. Littlefield, A. J. Logsdail, K. Lopata, W. Ma, A. V. Marenich, J. M. del Campo, D. Mejia-Rodriguez, J. E. Moore, J. M. Mullin, T. Nakajima, D. R. Nascimento, J. A. Nichols, P. J. Nichols, J. Nieplocha, A. Otero-de-la-Roza, B. Palmer, A. Panyala, T. Pirojsirikul, B. Peng, R. Peverati, J. Pittner, L. Pollack, R. M. Richard, P. Sadayappan, G. C. Schatz, W. A. Shelton, D. W. Silverstein, D. M. A. Smith, T. A. Soares, D. Song, M. Swart, H. L. Taylor, G. S. Thomas, V. Tipparaju, D. G. Truhlar, K. Tsemekhman, T. Van Voorhis, A. Vásquez-Mayagoitia, P. Verma, O. Villa, A. Vishnu, K. D. Vogiatzis, D. Wang, J. H. Weare, M. J. Williamson, T. L. Windus, K. Woliński, A. T. Wong, Q. Wu, C. Yang, Q. Yu, M. Zaharias, Z. Zhang, Y. Zhao, and R. J. Harrison, "NWChem: Past, present, and future," J. Chem. Phys. **152**, 184102 (2020).
[89]A. D. Becke, "A new mixing of Hartree–Fock and local density-functional theories," J. Chem. Phys. **98**, 1372–1377 (1993).
[90]A. Schäfer, H. Horn, and R. Ahlrichs, "Fully optimized contracted Gaussian basis sets for atoms Li to Kr," J. Chem. Phys. **97**, 2571–2577 (1992).
[91]T. H. Dunning, Jr. and F. J. Hay, "Gaussian basis sets for molecular calculations," in *Methods of Electronic Structure Theory*, *Modern Theoretical Chemistry Vol. 3*, edited by H. F. Schaefer III (Springer Science+Business Media, 1977), Chap. 1, pp. 1–28.
[92]P. Elliott, F. Furche, and K. Burke, "Excited states from time-dependent density functional theory," in *Reviews in Computational Chemistry*, edited by K. B. Lipkowitz and T. R. Cundari (Wiley-VCH, 2009), Chap. 3, pp. 91–165.
[93]M. Gronowski, "TD-DFT benchmark: Excited states of atoms and atomic ions," Comput. Theor. Chem. **1108**, 50–56 (2017).
[94]D. Escudero, A. D. Laurent, and D. Jacquemin, "Time-dependent density functional theory: A tool to explore excited states," in *Handbook of Computational Chemistry*, 2nd ed., edited by J. Leszczynski, A. Kaczmarek-Kedziera, T. Puzyn, M. G. Papadopoulos, H. Reis, and M. K. Shukla (Springer International Publishing, 2017), Chap. 21, pp. 927–961.
[95]J. Liang, X. Feng, D. Hait, and M. Head-Gordon, "Revisiting the performance of time-dependent density functional theory for electronic excitations: Assessment of 43 popular and recently developed functionals from rungs one to four," J. Chem. Theory Comput. **18**, 3460–3473 (2022).
[96]V. Mahamiya, P. Bhattacharyya, and A. Shukla, "Benchmarking Gaussian basis sets in quantum-chemical calculations of photoabsorption spectra of light atomic clusters," ACS Omega **7**, 48261–48271 (2022).
[97]F. M. F. de Groot, M. Grioni, J. C. Fuggle, J. Ghijsen, G. A. Sawatzky, and H. Petersen, "Oxygen 1*s* x-ray-absorption edges of transition-metal oxides," Phys. Rev. B **40**, 5715–5723 (1989).
[98]A. P. Hitchcock and C. E. Brion, "Inner-shell excitation of formaldehyde, acetaldehyde and acetone studied by electron impact," J. Electron Spectrosc. Relat. Phenom. **19**, 231–250 (1980).
[99]M. B. Robin, I. Ishii, R. McLaren, and A. P. Hitchcock, "Fluorination effects on the inner-shell spectra of unsaturated molecules," J. Electron Spectrosc. Relat. Phenom. **47**, 53–92 (1988).
[100]A. P. Hitchcock, S. G. Urquhart, and E. G. Rightor, "Inner-shell spectroscopy of benzaldehyde, terephthalaldehyde, ethylbenzoate, terephthaloyl chloride and phosgene: Models for core excitation of poly(ethylene terephthalate)," J. Phys. Chem. **96**, 8736–8750 (1992).
[101]S. G. Urquhart and H. Ade, "Trends in the carbonyl core (C 1S, O 1S) $\rightarrow \pi^*_{C=O}$ transition in the near-edge X-ray absorption fine structure spectra of organic molecules," J. Phys. Chem. B **106**, 8531–8538 (2002).
[102]I. Ishii and A. P. Hitchcock, "The oscillator strengths for C1s and O1s excitation of some saturated and unsaturated organic alcohols, acids and esters," J. Electron Spectrosc. Relat. Phenom. **46**, 55–84 (1988).
[103]S. G. Urquhart, A. P. Hitchcock, R. D. Priester, and E. G. Rightor, "Analysis of polyurethanes using core excitation spectroscopy. Part II: Inner shell spectra of ether, urea and carbamate model compounds," J. Polym. Sci., Part B: Polym. Phys. **33**, 1603–1620 (1995).
[104]V. Feyer, O. Plekan, R. Richter, M. Coreno, K. C. Prince, and V. Carravetta, "Core level study of alanine and threonine," J. Phys. Chem. A **112**, 7806–7815 (2008).
[105]O. Plekan, V. Feyer, R. Richter, M. Coreno, M. de Simone, K. C. Prince, and V. Carravetta, "An X-ray absorption study of glycine, methionine and proline," J. Electron Spectrosc. Relat. Phenom. **155**, 47–53 (2007).
[106]S. Bodeur, P. Millié, and I. Nenner, "Single- and multiple-electron effects in the Si 1s photoabsorption spectra of SiX_4 (X = H, D, F, Cl, Br, CH_3, C_2H_5, OCH_3, OC_2H_5) molecules: Experiment and theory," Phys. Rev. A **41**, 252–263 (1990).
[107]R. G. Cavell and A. Jürgensen, "Chemical shifts in P-1s photoabsorption spectra of gaseous phosphorus compounds," J. Electron Spectrosc. Relat. Phenom. **101–103**, 125–129 (1999).
[108]S. Bodeur and J. M. Esteva, "Photoabsorption spectra of H_2S, CH_3SH and SO_2 near the sulfur K edge," Chem. Phys. **100**, 415–427 (1985).
[109]M. J. Hanus and E. Gilberg, "The K absorption spectra of chlorine in gaseous CH_3Cl, C_2H_5Cl, CF_2Cl_2, and C_2H_3Cl," J. Phys. B: At. Mol. Phys. **9**, 137–145 (1976).
[110]X-ray Transition Energies database https://physics.nist.gov/PhysRefData/XrayTrans/Html/search.html; accessed 25 May 2024.
[111]S. S. Crawford and H. D. Kaesz, "Metalation reactions. 12. Metalation of acetyl- and dimethylaminomethylferrocenes with pentacarbonyl(methyl)manganese or -rhenium: Formation of homoannular metalated ferrocenes and ferrocenylmethylaminomethyl(tetracarbonyl)manganese," Inorg. Chem. **16**, 3193–3201 (1977).
[112]D. Scapens, H. Adams, T. R. Johnson, B. E. Mann, P. Sawle, R. Aquil, T. Perrior, and R. Motterlini, "[(η-C_5H_4R)Fe(CO)$_2$X], X = Cl, Br, I, NO_3, CO_2Me and [(η-C_5H_4R)Fe(CO)$_3$]$^+$, R = $(CH_2)_nCO_2Me$ (n = 0–2), and $CO_2CH_2CH_2OH$: A new group of CO-releasing molecules," Dalton Trans. **2007**, 4962–4973.
[113]H. Luth, E. A. Hall, W. A. Spofford, and E. L. Amma, "The crystal and molecular structure of bis(dithiobiureto)nickel(II)," J. Chem. Soc. D **1969**, 520–521.
[114]B. R. M. Lake and C. E. Willans, "Structural diversity of copper(I)–N-heterocyclic carbene complexes; ligand tuning facilitates isolation of the first structurally characterised copper(I)–NHC containing a copper(I)–alkene interaction," Chem. - Eur. J. **19**, 16780–16790 (2013).
[115]D. Balcells and B. B. Skjelstad, "tmQM dataset—quantum geometries and properties of 86k transition metal complexes," J. Chem. Inf. Model. **60**, 6135–6146 (2020).
[116]A. Kubas, M. Verkamp, J. Vura-Weis, F. Neese, and D. Maganas, "Restricted open-shell configuration interaction singles study on M- and L-edge x-ray absorption spectroscopy of solid chemical systems," J. Chem. Theory Comput. **14**, 4320–4334 (2018).
[117]D. E. Woon and T. H. Dunning, Jr., "Gaussian basis sets for use in correlated molecular calculations. V. Core-valence basis sets for boron through neon," J. Chem. Phys. **103**, 4572–4585 (1995).
[118]T. M. Willey, J. R. I. Lee, D. Brehmer, O. A. P. Mellone, L. Landt, P. R. Schreiner, A. A. Fokin, B. A. Tkachenko, A. de Meijere, S. Kozhushkov, and

A. W. van Buuren, "X-ray spectroscopic identification of strain and structure-based resonances in a series of saturated carbon-cage molecules: Adamantane, twistane, octahedrane, and cubane," J. Vac. Sci. Technol., A **39**, 053208 (2021).
[119]M. Cini, T. D. Bradshaw, and S. Woodward, "Using titanium complexes to defeat cancer: The view from the shoulders of titans," Chem. Soc. Rev. **46**, 1040–1051 (2017).
[120]R. Mayer, D. W. Lindle, S. H. Southworth, and P. L. Cowan, "Direct determination of molecular orbital symmetry of H_2S using polarized x-ray emission," Phys. Rev. A **43**, 235–241 (1991).
[121]D. W. Lindle, P. L. Cowan, T. Jach, R. E. LaVilla, R. D. Deslattes, and R. C. C. Perera, "Polarized x-ray emission studies of methyl chloride and the chlorofluoromethanes," Phys. Rev. A **43**, 2353–2366 (1991).
[122]A. E. A. Fouda and N. A. Besley, "Assessment of basis sets for density functional theory-based calculations of core-electron spectroscopies," Theor. Chem. Acc. **137**, 6 (2018).
[123]R. Sarangi, M. L. Vidal, S. Coriani, and A. I. Krylov, "On the basis set selection for calculations of core-level states: Different strategies to balance cost and accuracy," Mol. Phys. **118**, e1769872 (2020).
[124]M. A. Ambroise, A. Dreuw, and F. Jensen, "Probing basis set requirements for calculating core ionization and core excitation spectra using correlated wave function methods," J. Chem. Theory Comput. **17**, 2832–2842 (2021).
[125]I. P. E. Roper and N. A. Besley, "The effect of basis set and exchange-correlation functional on time-dependent density functional theory calculations within the Tamm-Dancoff approximation of the x-ray emission spectroscopy of transition metal complexes," J. Chem. Phys. **144**, 114104 (2016).
[126]Uncontraction should be done carefully since cc-pCVXZ basis sets use the same primitive Gaussians for several different contracted Gaussians. The same primitives should not be repeated in the uncontracted basis set.
[127]A. Bussy and J. Hutter, "Efficient and low-scaling linear-response time-dependent density functional theory implementation for core-level spectroscopy of large and periodic systems," Phys. Chem. Chem. Phys. **23**, 4736–4746 (2021).
[128]S. Pak and D. R. Nascimento, "The role of the coupling matrix elements in time-dependent density functional theory on the simulation of core-level spectra of transition metal complexes," Electron. Struct. **6**, 015014 (2024).
[129]Ohio Supercomputer Center http://osc.edu/ark:/19495/f5s1ph73; accessed 25 May 2024.